PAPER

Photoluminescence quenching of inorganic cesium lead halides perovskite quantum dots (CsPbX₃) by electron/hole acceptor†

Yan-Xia Zhang, Hai-Yu Wang,* Zhen-Yu Zhang, Yu Zhang, Chun Sun, Yuan-Yuan Yue, Lei Wang, Qi-Dai Chen and Hong-Bo Sun

Recently, all-inorganic cesium lead halide perovskites (CsPbX$_3$) quantum dots (QDs) have attracted great attention due to their halogen composition and size tunable band gap engineering, the same physical mechanism that is responsible for excellent performance in light-emitting devices. However, little is known about the time-resolved fluorescence quenching dynamics process of these CsPbX$_3$ QDs. In this article, we present comprehensive contrastive spectral studies on the electron and hole extraction dynamics of CsPbX$_3$ colloidal QDs with and without quencher by time-resolved femtosecond transient absorption (TA) and time-correlated single-photon counting (TCSPC) spectroscopy methods. We have identified that the partial electrons of the conduction band and holes of the valence band of CsPbX$_3$ QDs can be directly extracted by tetracyanoethylene (TCNE) and phenothiazine (PTZ), respectively. Moreover, compared with the CsPbBr$_3$ QDs, the CsPbI$_3$ QDs showed relatively slower charge extraction rates. We also found that the CsPbBr$_3$ QDs with smaller size showed faster carrier recombination rates and photoluminescence (PL) decay lifetime due to the relatively stronger quantum confinement effects. We believe that this study may be useful for realising optimal applications in photovoltaic and light emission devices.

Introduction

Organic–inorganic hybrid halide perovskites have been studied since 2009; however, only in the last five years has the vast potential of this material come to light.[1] Due to excellent optical and electronic properties, this material can be used for both photovoltaic applications[2] and light-emitting devices.[3] Generally speaking, perovskite materials have the same crystal structure as calcium titanate (CaTiO$_3$) and the chemical formula ABX$_3$, in which the A site is conventionally occupied by an organic cation such as CH$_3$NH$_3^+$, B site is usually occupied by a divalent metal ion such as Pb^{2+} and the X site is occupied by a halide ion (such as Cl$^-$, Br$^-$ or I$^-$).[4] They have been widely used in many fields, such as in biological environments, solar cells, organic light-emitting diodes (OLED) and single-photon sources.[5–7] These hybrid organic–inorganic CH$_3$NH$_3$PbBr$_3$ QDs show a very favorable size-dependent quantum confinement effects with enhanced optical properties compared with bulk counterparts, such as high PL quantum yields (PLQYs) and

high-purity narrow-band emission. However, these organic–inorganic halide perovskites are very sensitive to oxygen and water, which prevent it from practical application in the real world. Fortunately, recent studies have provided new perovskite QDs, *i.e.*, inorganic CsPbX$_3$ QDs with a cubic shape or cubic perovskite crystal nanostructures.[8–10] In addition to its stability, CsPbX$_3$ QDs exhibits a size-tunable compositional band-gap transition throughout the entire visible spectral region. In terms of the optoelectronic properties, though few studies have involved the fluorescence characteristic of CsPbX$_3$ QDs, the knowledge of the PL quenching and charge transfer processes in QDs is still unclear.[11]

In this study, steady state and time-resolved TA and PL spectroscopy experiments were carried out to investigate charge carrier transfers and the PL quenching process of CsPbX$_3$ QDs when different concentrations of TCNE and PTZ were added. Particularly, the femtosecond TA spectroscopic technique was widely used to investigate the ultrafast dynamic evolution of photoexcited carriers in various types of materials. Transient TA dynamics is mainly determined by the temporal change in carrier density. This spectroscopic technique will be highly effective for achieving more precise and fundamental understandings of the quenching mechanism in halide perovskites QDs. The details will be discussed in the following sections.

State Key Laboratory on Integrated Optoelectronics, College of Electronic Science and Engineering, Jilin University, 2699 Qianjin Street, Changchun 130012, China. E-mail: haiyu_wang@jlu.edu.cn

Experimental

In the present study CsPbX$_3$ quantum dots were prepared as per the following steps. First, Cs$_2$CO$_3$ (0.814 g), octadecene (40 mL, ODE) and oleic acid (2.5 mL, OA) were mixed in a 100 mL 3-neck flask, dried in vacuum for 1 h at 120 °C, and then heated under N$_2$ to 150 °C until all Cs$_2$CO$_3$ reacted with OA and ODE. Since Cs-oleate could be easily precipitated from ODE at room-temperature, it had to be pre-heated to 100 °C before injection. Second, ODE (10 mL), PbBr$_2$ (0.138 g) or PbI$_2$ (0.104 g), dried oleylamine (1 mL, OLA) and dried OA (1 mL) were loaded into a 50 mL 3-neck flask and dried at 120 °C under N$_2$. After the PbX$_2$ salt was completely dissolved, the temperature was raised to 140–200 °C (for tuning the QD size) and Cs-oleate solution (0.8 mL, prepared as described above) was quickly injected and, 5 s later, the reaction mixture was cooled using an ice-water bath. Finally, aggregated quantum dots were separated by centrifuging. After centrifugation, the supernatant was filtered and the aggregated QDs were dissolved in toluene solutions.[12] The femtosecond TA system are set up as follows. A beam splitter split an 800 nm pulse (100 fs, 250 Hz repetition rate) from the amplifier into two parts to produce a pump pulse and a probe pulse. The 400 nm pump pulse was obtained by a beta barium borate (BBO) crystal. The frequency of the 400 nm pulse came to 125 Hz by passing a chopper. The continuous white-light probe pulses from 400 nm to 850 nm were achieved by using an 800 nm laser to excite the 2 mm thick reservoir in the cuvette. Time-resolved TA spectra were recorded with a highly sensitive spectrometer. The dynamic traces were obtained by controlling the relative delay between the pump and the probe pulses by a stepper-motor-driven optical delay line.[13]

Results and discussion

Fig. 1a shows the absorption (red) and emission (green) spectra of CsPbBr$_3$ QDs. The absorption spectrum has a band edge at 505 nm and the PL spectrum possesses a sharp emission peak at 520 nm. The absorption spectra of CsPbI$_3$ QDs shown in Fig. 1c has the band edge at 673 nm and shows the corresponding narrow emission PL spectrum at 700 nm. We hold that PL origin is the band-to-band radiative recombination of the electrons at the conduction band and the holes at the valence band. In order to analyze the phase structure, we investigated the perovskite QDs morphology with high-resolution transmission electron microscopy (HRTEM) using the JEM-2100F transmission electron microscope. Fig. 1b and d show the representative TEM images of CsPbX$_3$ QDs as well as the size distribution; it was observed that typical CsPbX$_3$ QDs had an average diameter of 15 nm with a normal cubic shape.

We chose two types of quenchers; TCNE acts as an electron acceptor and PTZ as a hole acceptor, respectively. First, TCNE and PTZ could be well dissolved in toluene; this is to say, quenching agents could be easily adsorbed onto CsPbX$_3$ QDs. Second, they are nonfluorescent, and hence they may act as dark quenchers, showing an extended advantage in terms of no interference with the fluorescence of QDs during the PL
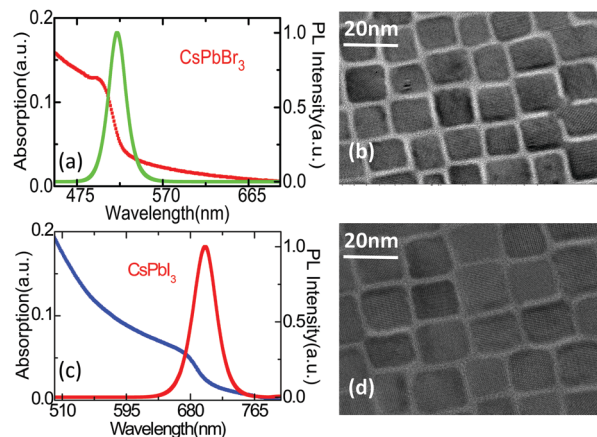

Fig. 1 (a) Absorption (red line) and PL (green line) spectrum of typical CsPbBr$_3$ perovskite QDs. (b) TEM image of CsPbBr$_3$ QDs. (c) Absorption (blue line) and PL (red line) spectrum of pure CsPbI$_3$ perovskite quantum dots. (d) TEM image of CsPbI$_3$ QDs.

quenching process. Herein, we introduce the energy diagrams of the QDs and the PL quenchers. As shown in Fig. 2a and b, we plotted the quenching process of QDs in different halogen cases for their different energy level structures and in different size cases for its quantum size effects. According to previous reports, the relative energy of the valence and conduction band edges of the QDs, and the reduction and oxidation potentials of quenchers (TCNE and PTZ) are certainly important, as they dictate the dicing force for the charge transfer processes.[13–15] All the abovementioned properties make TCNE and PTZ the most suitable quenching agents in our experiments. As shown in Fig. 2, the partial electrons and holes will be extracted by TCNE and PTZ, respectively. Then, the remaining electrons and holes will recombine to the valence and conduction bands, respectively. As we all know, fluorescence quenching refers to any process that decreases the fluorescence intensity of a given substance. A variety of processes can result in quenching, such as excited state reactions, energy transfer, complex-formation and collisional quenching.[16] Pure static quenching involves ground-state complex formation between the donor (fluorophore) and acceptor (quencher), which is accompanied by changes in the donor absorption features in the donor/acceptor mixture.[17]

Fig. 3a and d, show the steady-state absorption spectra of CsPbBr$_3$ and CsPbI$_3$ QDs adsorbed with quenchers, respectively.
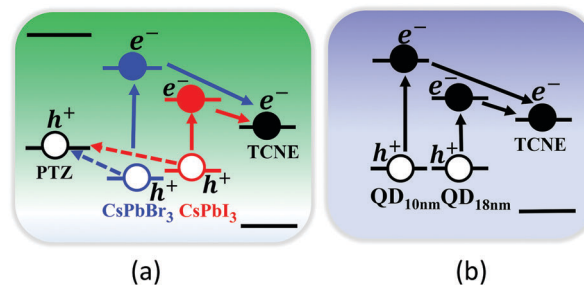

Fig. 2 Halogen-dependent (a) and size-dependent (b) energy levels diagram of bare QDs and the QDs–quenchers complexes.

This journal is © the Owner Societies 2017

Phys. Chem. Chem. Phys., 2017, 19, 1920–1926 | 1921

The interband absorptions are centered at 505 and 673 nm. It is well known that the pure static quenching involves ground-state complex formation between donor (fluorophore) and acceptor (quencher), which is accompanied by changes in the absorption features of the donor in the donor/acceptor mixture. However, in this study, the absence of perturbations of bare QDs absorption features and the non-appearance of any extra absorption band ruled out the possibility of pure static quenching. All the samples possess the same absorption range from the ultraviolet to visible light, exhibiting the same absorption line-style, and we assigned it to the excitonic transition.[18]

Fig. 3b and c show the steady-state 400 nm laser excited emission spectra of $CsPbBr_3$ QDs dissolved in different concentrations of TCNE and PTZ, respectively. Interestingly, it was observed that the increasing concentration of quencher led to a gradual decrease of the PL intensity for the bare QDs, clearly indicating the enhanced quenching effects due to the increased densities of TCNE and PTZ. The quenched fluorescence of the $CsPbBr_3$ QDs doped with quencher indicated that the quencher molecules had been successfully affiliated to the bare $CsPbBr_3$ QDs surfaces. Based on this, the excited electron in the $CsPbBr_3$ QDs transitioned to the TCNE and the hole transitioned to the PTZ.[19] We also checked for the PL quenching effects of $CsPbI_3$ QDs. As shown in Fig. 3e and f, similar to $CsPbBr_3$ QDs, the fluorescence intensities of steady-state PL at 700 nm of $CsPbI_3$ QDs also decreased when the TCNE and PTZ concentrations were increased.
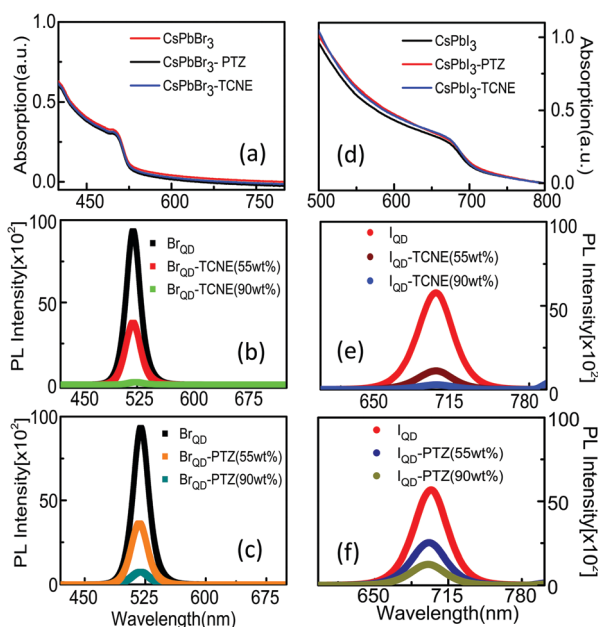

Fig. 4 (a) Time-resolved TA spectra of $CsPbBr_3$ QDs with sizes of 18 nm, $CsPbBr_3$ adsorbed with 55% TCNE (b) and $CsPbBr_3$ adsorbed with 55% PTZ (c). (d) Time-resolved TA spectra of $CsPbI_3$ QDs, $CsPbI_3$ adsorbed with 55% TCNE (e) and $CsPbI_3$ adsorbed with 55% PTZ (f). The time-resolved TA spectra were obtained at different probe delay times following 400 nm laser excitation with an energy density of 21.5 μJ cm^{-2}. Arrows indicate transient bleach recovery.

In order to investigate these ultrafast dynamics of the quenching process, 400 nm excited time-resolved femtosecond TA experiments was carried out on these samples, and these results are presented in Fig. 4 and 5. The pumped intensities were fixed at 21.5 μJ cm^{-2}. Usually, three types of spectral signals could be observed in the TA spectra. During the pumping experiments, these carriers excited by the pump light will follow the Pauli exclusion principle. The filling of electronic states will lead to the negative TA bleaching signals, namely, the corresponding optical transitions from the ground state to the excited state, which is called ground-state bleaching (GBS).[20-22] The photoexcited electrons in the excited states could further absorb probe light and leap onto higher energy levels or return to the ground state by stimulated radiation because of the interference of the probe light, which is called the excited-state absorption (ESA) and stimulated emission (SE), respectively. ESA possessed positive signals, whereas SE had negative signals. All these signals reflect the change of photo-generated carrier populations in the corresponding energy levels.

Fig. 4a–c show the typical time-resolved TA spectra of bare $CsPbBr_3$ QDs and $CsPbBr_3$ QDs adsorbed with TCNE (55 wt%) and PTZ (55 wt%), respectively. All these spectra show an identical sharp negative signal at 505 nm, which corresponds to the energy band structure confirmed by the steady-state absorption spectrum experiments. The shape of the spectrum was independent of delay time, pump intensity and quencher concentration. The bleaching-signal intensity reflects the band-edge photocarrier density. The bleaching intensity of $CsPbBr_3$ QD–TCNE and $CsPbBr_3$ QD–PTZ complex was much smaller

Fig. 3 (a) Absorption spectra of pure $CsPbBr_3$ QDs, $CsPbBr_3$ QDs adsorbed with TCNE and $CsPbBr_3$ QDs adsorbed with PTZ. (b) The steady-state PL spectra of $CsPbBr_3$ QDs solution with addition of 55 wt% TCNE and 90 wt% TCNE. (c) The steady-state PL spectra of $CsPbBr_3$ QDs solution with addition of 55 wt% PTZ and 90 wt% PTZ. (d) Absorption of pure $CsPbI_3$ QDs, $CsPbI_3$–PTZ and $CsPbI_3$–TCNE. (e) The steady-state PL spectra of $CsPbI_3$ QDs solution upon the addition of 55 wt% TCNE and 90 wt% TCNE. (f) The steady-state PL spectra of $CsPbI_3$ QDs solution upon the addition of 55 wt% PTZ and 90 wt% PTZ.
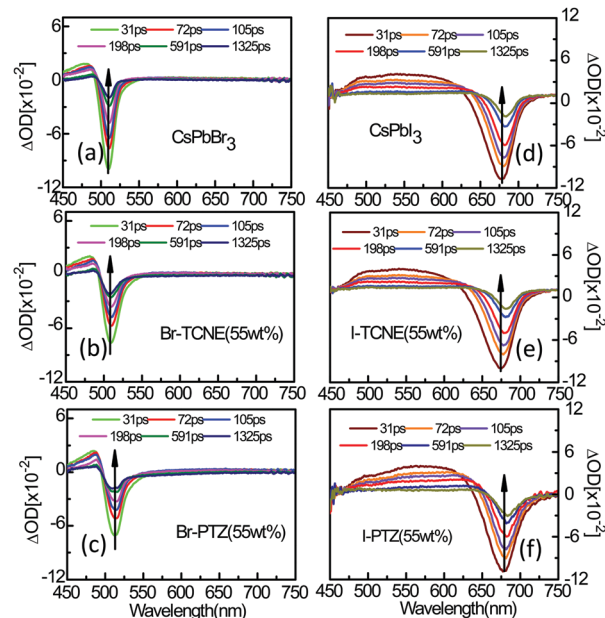
1922 | Phys. Chem. Chem. Phys., 2017, 19, 1920–1926

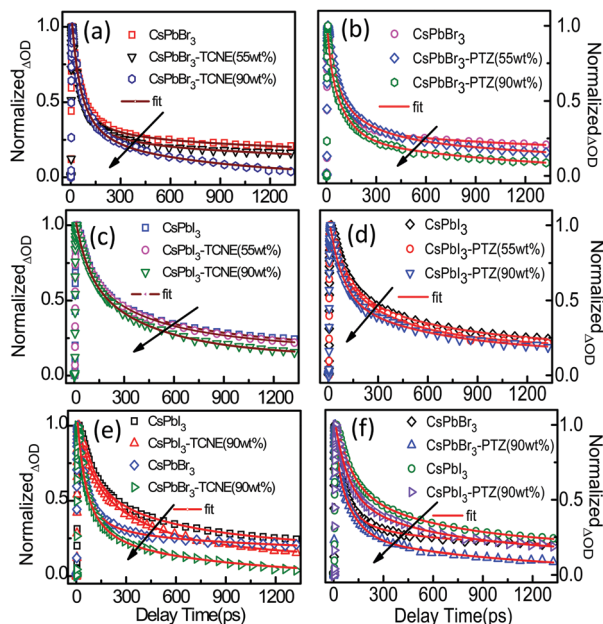This journal is © the Owner Societies 2017

Fig. 5 (a) Kinetic profiles of 505 nm transient bleach recovery of CsPbBr$_3$ QDs, CsPbBr$_3$ − 55 wt% TCNE and CsPbBr$_3$ − 90 wt% TCNE. (b) Kinetic profiles of 505 nm transient bleach recovery of CsPbBr$_3$ QDs, CsPbBr$_3$ − 55 wt% PTZ and CsPbBr$_3$ − 90 wt% PTZ. (c) Kinetic profiles of 673 nm transient bleach recovery of CsPbI$_3$ QDs, CsPbI$_3$ − 55 wt% TCNE and CsPbI$_3$ − 90 wt% TCNE. (d) Kinetic profiles of 505 nm transient bleach recovery of CsPbI$_3$ QDs, CsPbI$_3$ 55 wt% PTZ and CsPbI$_3$ − 90 wt% PTZ. (e) The transient band edge bleach kinetics for CsPbBr$_3$ QDs, CsPbBr$_3$ − 90 wt% TCNE, CsPbI$_3$ QDs and CsPbI$_3$ − 90 wt% TCNE. (f) The transient band edge bleach kinetics for CsPbBr$_3$ QDs, CsPbBr$_3$ − 90 wt% PTZ, CsPbI$_3$ QDs and CsPbI$_3$ − 90 wt% PTZ. For different Halide QDs, the charge transfer rate of CsPbI$_3$ adsorbed with quencher (TCNE or PTZ) is lower.

than that of the bare CsPbBr$_3$ QDs under the same experimental conditions. This changing of the bleaching intensity indicates that their quantities were decreased. Hence, we can ensure that the TCNE and PTZ have effectively extracted the electrons and holes from the conductance and valance bands, respectively. The TA spectra of CsPbBr$_3$ QDs–TCNE (90 wt%), CsPbBr$_3$ QDs–PTZ (90 wt%) are shown in Fig. S1a and b (ESI†). At the same time, Fig. 4d–f show the typical time-resolved TA spectra of bare CsPbI$_3$ QDs, CsPbI$_3$ QDs adsorbed with TCNE (55 wt%) and PTZ (55 wt%), respectively. The position of negative GBS was confirmed at 673 nm; moreover, red shifting compared with the CsPbBr$_3$ QDs and the bleaching magnitude of the CsPbI$_3$ QDs–TCNE and CsPbI$_3$ QDs–PTZ was also respectively decreased.

Fig. 5a and b compare the band edge transition dynamics (505 nm) of the bare CsPbBr$_3$ QDs with their complexes adsorbed onto TCNE and PTZ, respectively. The modulation of the decay kinetics was previously attributed to Auger recombination in quantum dots. It can be seen that the kinetic recombination rates became faster with increasing quencher concentration from these spectrogram. The faster recombination rates clearly indicated that the electron and hole were transferred from CsPbBr$_3$ QDs to TCNE and PTZ, respectively. We attributed this phenomenon to the fast charge transfer, as the bare CsPbBr$_3$ QDs inhibit the transfer process. It can also be

observed that the charge transfer rate of CsPbI$_3$ QDs adsorbed with quencher is a little faster than the bare CsPbI$_3$ QDs, which is shown in Fig. 5c and d. In order to study the influence of different halogens on the charge transfer rates of CsPbX$_3$ QDs, in Fig. 4e and f, we compared the quenching kinetics of CsPbI$_3$ QDs and CsPbBr$_3$ QDs compared with their complexes adsorbed to TCNE and PTZ, respectively. It can be concluded that the carriers decay rate of CsPbBr$_3$ QDs is much higher than that of the CsPbI$_3$ QDs due to the different energy level. In the presence of a quenching agent (TCNE and PTZ), the carrier transfer rates of the CsPbBr$_3$ QDs–quencher complexes are also much faster than for the CsPbI$_3$ QDs–quencher complexes. This phenomenon can be attributed to the greater difference of energy levels in the CsPbI$_3$ QDs, which caused the charge transfer rate to increase. The detailed fitting information is shown in Table S1 (ESI†).

In order to define the different perovskite lattices' characteristics, we performed XRD (X-ray diffraction) measurements of CsPbBr$_3$ and CsPbI$_3$ QDs, and the results are shown in Fig. 6a. As shown in the XRD spectra in Fig. 6a, the three main perovskite peaks at 15.01°, 21.37° and 30.30° corresponding to the (110), (220) and (330) diffractions of perovskite cubic CsPbBr$_3$ QDs can be readily read. Due to the different halogens, the cubic CsPbI$_3$ QDs show blue-shifted XRD peaks at 14.48°, 20.51° and 28.98° respectively. These XRD peaks are similar to those published previously[12] and confirm that these cubic QDs are indeed well fabricated. In order to obtain a deeper understanding of the radiate recombination dynamical behavior of the photocarriers,[23] the PL decay traces of these excited samples were confirmed by the TCSPC system using single-channel method, pumped with a 405 nm picosecond diode laser (Edinburgh Instruments EPL405, repetition rate 20 MHz). Normalized PL decay traces of bare CsPbBr$_3$ QDs and CsPbI$_3$ QDs–quencher complexes are shown in Fig. 6b. The black line illustrates the PL decay process of bare CsPbBr$_3$ QDs and others present the quenched dynamics of CsPbBr$_3$ QDs–quencher complexes. Generally speaking, the CsPbBr$_3$ QDs excited state
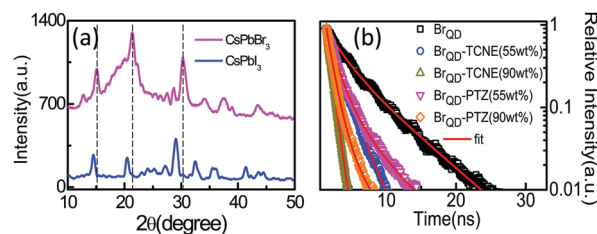
(c) Sample	τ_1/ns	τ_2/ns	τ_{ave}/ns
CsPbBr$_3$	7.78(100%)	0	7.78
Br$_{QD}$-PTZ(55wt%)	2.62(82%)	8.3(18%)	3.58
Br$_{QD}$-PTZ(90wt%)	2.03(88%)	10.32 (12%)	2.98
Br$_{QD}$-TCNE(55wt%)	1.16(75%)	8.83(25%)	3.42
Br$_{QD}$-TCNE(90wt%)	1.22(96%)	4.81(14%)	1.34

Fig. 6 (a) XRD patterns for CsPbBr$_3$ QDs and CsPbI$_3$ QDs. (b) Time-resolved PL decays for pure CsPbBr$_3$ QDs, CsPbBr$_3$ QDs dissolved in 55 wt% TCNE, 90 wt% TCNE, 55 wt% PTZ and 90 wt% PTZ respectively. (c) Best-fit parameters of time-resolved PL decays for all samples shown in (b).

recombination will lead to a multiexponential PL decay profile, which can be expressed as follows:

$$I_{(t)} = \sum_{i=0}^{n} \alpha_i \exp(-t/\tau_i)$$

where n is number of decay components, α_i and τ_i are the amplitude and the decay time of the ith component, respectively. The amplitudes of the decay components reflect the total contribution of each lifetime component toward the average lifetime. Therefore, from the amplitude and the corresponding lifetime component (fitted in Fig. 6c), the average lifetime $\langle \tau_{\text{avg}} \rangle$ can be calculated as follows:

$$\langle \tau_{\text{avg}} \rangle = \sum \alpha_i \tau_i^2 \Big/ \sum \alpha_i \tau_i$$

From Fig. 6c, we learned that the PL lifetime of CsPbBr$_3$ QDs was 7.78 ns, and the PL lifetime of CsPbBr$_3$ QDs dissolved in TCNE (55 wt%) solution was 3.42 ns, whereas that in TCNE (90 wt%) solution was 1.34 ns. We can clearly see that the PL lifetimes of CsPbBr$_3$ QDs adsorbed with quenchers (TCNE and PTZ) became faster and the effects became more dominating with increased quencher concentration. Generally, the fluorescence intensity decay was consistent with the law of exponential decay and the corresponding equations are as follows:

$$I_{\text{without}} = I_0 \int e^{-k_0 t} dt \qquad (1)$$

$$I_{\text{with}} = I_0 \int e^{-(k_0 + k_q)t} dt \qquad (2)$$

$$\tau_{\text{without}} = \frac{1}{k_0} \qquad (3)$$

$$\tau_{\text{with}} = \frac{1}{k_0 + k_q} \qquad (4)$$

where I_0 is the fluorescence intensity of bare CsPbBr$_3$ QDs, k_0 is the decay rate constant, k_q is the charge transfer rate, η is the quenching coefficient, the fluorescence lifetime is τ, and γ is the variation of the fluorescence lifetime. Herein, we explained the quenching process by analyzing the fluorescence decay lifetime of CsPbX$_3$ QDs and QDs–quencher complexes. Herein, we supposed that $I_{\text{without}}(I_{\text{w0}})$ and $\tau_{\text{without}}(\tau_0)$ stands for the fluorescence intensity and decay lifetime of bare CsPbBr$_3$ QDs, respectively; the fluorescence intensity and lifetime of CsPbBr$_3$ QDs–TCNE (55 wt%) are abbreviated as $I_{\text{without1}}(I_{\text{w1}})$ and $\tau_{\text{with1}}(\tau_{\text{w1}})$, whereas those of the CsPbBr$_3$ QDs–TCNE (90 wt%) are $I_{\text{without2}}(I_{\text{w2}})$ and $\tau_{\text{with2}}(\tau_{\text{w2}})$. Therefore, according to the following equations, we calculated the quenching coefficient and fluorescence variation.

$$\eta = 1 - \frac{I_{\text{with}}}{I_{\text{without}}}, \quad \eta_1 = 1 - \frac{I_{\text{w1}}}{I_{\text{w0}}} = 0.60, \quad \eta_2 = 1 - \frac{I_{\text{w2}}}{I_{\text{w0}}} = 0.85.$$

$$\gamma = 1 - \frac{I_{\text{with}}}{I_{\text{without}}}, \quad \gamma_1 = 1 - \frac{I_{\text{w1}}}{I_{\text{w0}}} = 0.56, \quad \gamma_2 = 1 - \frac{I_{\text{w2}}}{I_{\text{w0}}} = 0.82.$$

It is interesting that the value of η is almost equal to γ. Hence, by comparing with the results of TA, it can be concluded

that the process of PL quenching mainly occurs within the TCSPC experiments time frame. The quenching coefficient of bare CsPbX$_3$ QDs and QDs–quencher complexes with different quenchers concentration can be obtained in the steady-state PL spectra shown in Fig. 3, according to the abovementioned conclusions. The quenching coefficient of CsPbBr$_3$–PTZ (55 wt%) and CsPbBr$_3$–PTZ (90 wt%) was 0.6 and 0.92 respectively. The quenching coefficient of CsPbI$_3$–PTZ (55 wt%) and CsPbI$_3$–PTZ (90 wt%) was 0.55 and 0.88, respectively. Therefore, we can reasonably infer that the charge transfer rate of CsPbBr$_3$–PTZ was faster than CsPbI$_3$–PTZ by comparing the quenching coefficients. At the same time, the charge transfer rate of CsPbBr$_3$–TCNE was also faster than CsPbI$_3$–TCNE. These results are also in agreement with TA spectra.

In addition to the PL quenching of different halide perovskites QDs, we also studied the effect of sizes on the quenching process by time-resolved TCSPC and TA experiments. First, two different-sized CsPbBr$_3$ QDs were prepared by changing the reacting temperature at 130 °C and 180 °C, with 10 and 18 nm sizes, respectively. Fig. 7a and b show TEM micrographs of relatively small-sized CsPbBr$_3$ QDs as well as the size distribution, showing an average diameter of 10 nm. Fig. 7c and d show the TEM micrographs of relatively larger-sized CsPbBr$_3$ QDs as well as the size distribution, showing an average diameter of 18 nm. We investigated the steady-state optical properties of QD$_{10\text{nm}}$ and QD$_{18\text{nm}}$, and the results are shown in Fig. 6e. As is known, both absorption shoulders and fluorescence peaks of QD will be red-shifted with increasing particle diameter due to their quantum size effects. The solid lines represent the absorption
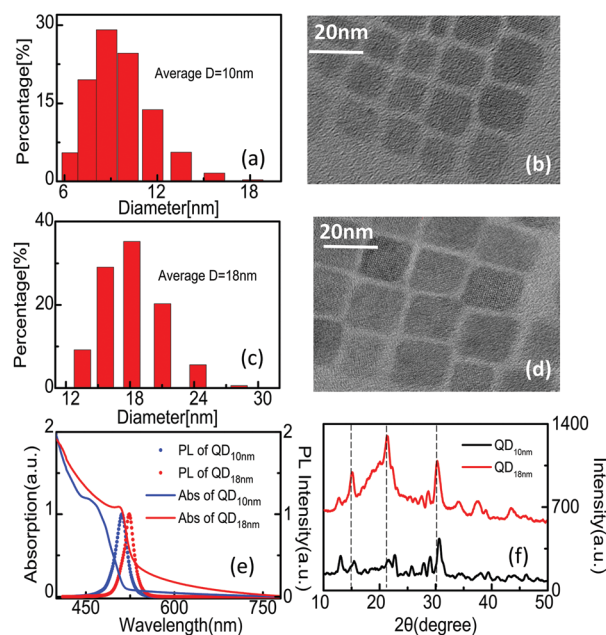

Fig. 7 (a) Size histogram of CsPbBr$_3$ QD$_{10\text{nm}}$ and (b) TEM images of CsPbBr$_3$ QD$_{10\text{nm}}$. (c) Size histogram of CsPbBr$_3$ QD$_{18\text{nm}}$ and (d) transmission electron micrographs of CsPbBr$_3$ QD$_{10\text{nm}}$. (e) Optical absorption (sold line), PL emission (PL, dash line) spectra of the spherical CsPbBr$_3$ quantum dots. Blue line stands the CsPbBr$_3$ QD$_{10\text{nm}}$, red one stands the CsPbBr$_3$ QD$_{18\text{nm}}$. (f) XRD patterns for CsPbBr$_3$ QD$_{10\text{nm}}$ (black) and CsPbBr$_3$ QD$_{18\text{nm}}$ (red).

spectra of QD_{10nm} (blue line) and QD_{18nm} (red line). The absorption shoulders of QD_{10nm} and QD_{18nm} appeared at 483 nm and 505 nm, respectively. We can also observed sharp emission peaks at 500 nm (QD_{10nm}) and 520 nm (QD_{18nm}) in the corresponding emission spectra (dashed line), respectively. Similar to Fig. 6a and 7f shows the X-ray diffraction (XRD) patterns of the QD_{10nm} and QD_{18nm}. Three main perovskite peaks at 15.01°, 21.37° and 30.30° corresponding to the (110), (220) and (330) diffractions of perovskite cubic $CsPbBr_3$ QDs can be readily observed. This spectrogram also indicated that the XRD patterns were independent of QD sizes.

In Fig. 8, we performed time-resolved femtosecond pump–probe measurements on QD_{10nm}, QD_{18nm} and QD–TCNE complex with 400 nm lasers with an identical intensity at 8.8 μJ cm^{-2}; after adjusting their absorption, intensity remains the same. From the point of view of TA spectra, shown in Fig. 8a and c, the GBS signal position of bare QD_{10nm} is at 483 nm and that of the QD_{18nm} is at 505 nm, which is in good agreement with the result from the UV-vis absorption spectra shown in Fig. 7e. The arrows indicate the location of the TA bleach signal. Fig. 8a and b show the TA spectra of QD_{10nm}–TCNE and QD_{18nm}–TCNE complexes, respectively, when the same amount of TCNE (90 wt%) was added to the bare QDs solutions. When the TCNE were added, the GBS positions of these spectra were not changed and we supposed that the additional ESA in Fig. 8b and d may be caused by the TCNE. Due to the smaller size of
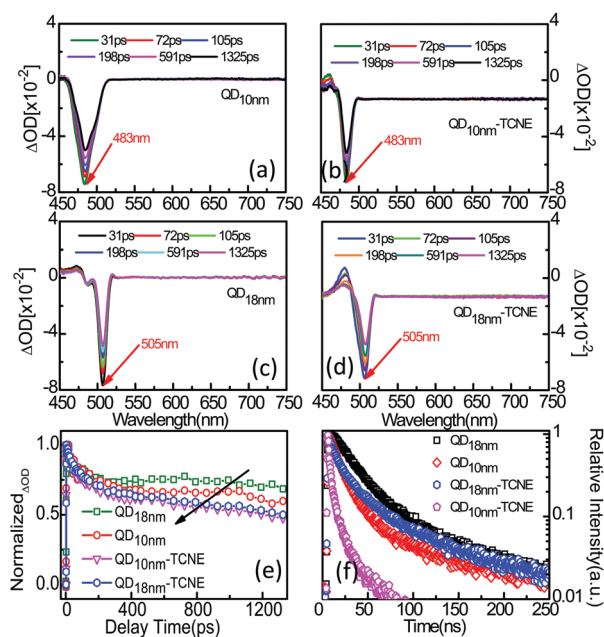
QDs relative to its exciton Bohr radius, the observed blue shifting of TA bleach signals could also be explained by the quantum confinement effect.[23,24] Moreover, similar to Fig. 4, the transient signals' intensities of QDs–TCNE were also reduced. The carriers decay kinetics of QD_{10nm}, QD_{18nm}, QD_{10nm}–TCNE and QD_{18nm}–TCNE complexes are shown in Fig. 8e. We found that the decay rate of QD_{10nm} was significantly faster compared to QD_{18nm}. In the presence of TCNE, the charge transfer rate of the QDs–TCNE complexes became faster than that of bare QDs. However, the charge transfer rate of QD_{18nm}–TCNE complexes was slightly slower compared to the QD_{10nm}–TCNE complexes. Additionally, due to decay rates of QDs being sensitively fluence-dependent: the decay rates will become more faster with increasing pump fluences. Therefore, the decay rates in Fig. 8e are much slower than those in Fig. 5.

In order to further investigate the effect of different sizes on fluorescence quenching. The time-resolved TCSPC PL decay spectra of these samples are shown in Fig. 7f. The average PL decay lifetimes of QDs–TCNE were also faster than those of bare QDs. Though the difference of energy gap between two sizes of quantum dots is not very large, it is interesting that the average decay lifetime of QD_{10nm}–TCNE is more different than that of QD_{18nm}–TCNE complexes. Clearly, QD_{10nm}–TCNE complexes show much faster decay rates. There are two major reasons for this phenomenon. First, it has been shown that, at low temperatures, this synthesis tends to produce lower symmetry structures such as nano-plates. Therefore, strictly speaking, the lattice structure of QD_{10nm} is not the pure cubic crystal structure. There is a possibility that some of the quenching effect that we observed may be accounted for by nanoplated that have different lifetimes and stronger exciton binding energy. Moreover, many previous reports also explained that fluorescence quenching of quantum dots is correlated with their surface states.[25] The surface to volume ratio difference between the two crystal sizes also leads to increased surface/quencher interactions in the smaller system.

As a necessary complement, Fig. S2a and b (ESI†) show the time-resolved femtosecond PL experiments performed under 400 nm excitation, to measure pure radiative recombination processes. All the fluorescence transients process were probed at the PL peaks and were well fitted with multiexponential functions shown in Table S2 (ESI†); the best-fit parameters are listed in Table S1 (ESI†). It is worth noticing that these average PL lifetimes only provide the information of relative emission strength. There is a fast decay trend compared to bare $CsPbBr_3$ QDs with $CsPbBr_3$ QDs adsorbed to TCNE and PTZ, respectively. The average PL lifetime became shorter after quenching. All of these samples had the same the increasing part, and therefore there is no hot electron injection. These time-resolved PL dynamics showed the same conclusions with TA.

Fig. 8 Time-resolved TA spectra of $CsPbBr_3$ QD_{10nm} (a), $CsPbBr_3$ QD_{10nm} adsorbed with TCNE (b), $CsPbBr_3$ QD_{18nm} (c) and $CsPbBr_3$ QD_{18nm} adsorbed with TCNE (d) at different probe delay times following 400 nm laser excitation with an 8.8 μJ cm^{-2} energy density. Red arrows indicate the location of transient bleach signals. (e) Transient band-edge bleaching kinetics at 483 nm ($CsPbBr_3$ QD_{10nm} and QD_{10nm}–TCNE) and 505 nm ($CsPbBr_3$ QD_{18nm} and QD_{18nm}–TCNE) after 400 nm excitation. Arrow indicates the kinetic trends. (f) Time-resolved PL decay of four samples with 375 nm excitation wavelength.

Conclusions

In conclusion, by utilizing time-resolved femtosecond TA and picosecond TCSPC technology, we have performed a comprehensive study on the mechanism of fluorescence quenching of

CsPbX$_3$ QDs, which includes TCNE and PTZ. We studied the PL quenching process of CsPbX$_3$ QDs adsorbed to quenchers with different concentrations. The results show that the quenching efficiencies of CsPbX$_3$ QDs are highly dependent on the concentration of TCNE and PTZ. Additionally, due to the difference of the energy levels with different halogens, CsPbI$_3$ QDs showed slower charge transfer rates than that of CsPbBr$_3$ QDs. The changing of fluorescence intensities of the bare QDs was consistent with the lifetime obtained by time-resolved TCSPC fluorescence experiments. At last, we also investigated that the effect of sizes on the CsPbBr$_3$ QDs fluorescence quenching caused by TCNE. Due to the difference of the surface state between the two sizes of CsPbBr$_3$ QDs, the fluorescence quenching efficiency and the charge transfer rate also showed significant size dependent properties. We believe that a deeper understanding of the PL quenching mechanism reported in this Letter may be good for optimizing the performance of perovskite QDs based light-emitting devices.

Acknowledgements

References

1 M. A. Green, A. H. Baillie and H. J. Snaith, *Nat. Photonics*, 2014, **8**, 506–514.
2 H. H. Fang, F. Wang, S. Adjokatse, N. Zhao, J. Even and M. A. Loi, *Light: Sci. Appl.*, 2016, **5**, e16056.
3 Z. K. Tan, R. S. Moghaddam, M. L. Lai, P. Docampo, R. H. Felix Deschler, M. Price, A. Sadhanala, L. M. Pazos, D. Credgington, F. Hanusch, H. J. Snaith and R. H. Friend, *Nat. Nanotechnol.*, 2014, **9**, 687–692.
4 S. D. Stranks, P. K. Nayak, W. Zhang, T. Stergiopoulos and H. J. Snaith, *Angew. Chem., Int. Ed.*, 2015, **54**, 3240–3248.
5 F. Zhang, H. Z. Zhong, C. Chen, X. G. Wu, X. M. Hu, H. L. Huang, J. B. Han, B. S. Zou and Y. P. Dong, *ACS Nano*, 2015, **9**, 4533–4542.
6 H. L. Huang, F. C. Zhao, L. G. Liu, F. Zhang, X. G. Wu, L. J. Shi, B. S. Zou, Q. B. Pei and H. Z. Zhong, *ACS Appl. Mater. Interfaces*, 2015, **7**, 28128–28133.
7 X. M. Li, Y. Wu, S. L. Zhang, B. Cai, Y. Gu, J. Z. Song and H. B. Zeng, *Adv. Mater.*, 2016, **15**, 2435–2445.
8 S. Sharma, N. Weiden and A. Weiss, *Z. Phys. Chem.*, 1992, **175**, 63–80.
9 D. M. Trots and S. V. Myagkota, *J. Phys. Chem. Solids*, 2008, **69**, 2520–2526.
10 C. C. Stoumpos, C. D. Malliakas and M. G. Kanatzidis, *Inorg. Chem.*, 2013, **52**, 9019–9038.
11 Y. F. Wang, H. Y. Wang, Z. S. Li, J. Zhao, L. Wang, Q. D. Chen and H. B. Sun, *J. Phys. Chem. C*, 2014, **118**, 17240–17246.
12 L. Protesescu, S. Yakunin, M. I. Bodnarchuk, F. Krieg, R. Caputo, C. H. Hendon and M. V. Kovalenko, *Nano Lett.*, 2015, **15**, 3692–3696.
13 D. Hanss, M. E. Walther and O. S. Wenger, *Chem. Commun.*, 2010, **46**, 7034–7036.
14 F. E. Stewart, M. Eisner and W. R. Carper, *J. Chem. Phys.*, 1966, **44**, 2866–2872.
15 P. Reutenauer, M. Kivala, P. D. Jarowski, C. Boudon, J. P. Gisselbrecht, M. Grossb and F. Diederich, *Chem. Commun.*, 2007, 4898–4900.
16 J. Huang, Z. Q. Huang, Y. Yang, H. M. Zhu and T. Q. Lian, *J. Am. Chem. Soc.*, 2010, **132**, 4858–4864.
17 A. Pal, S. Srivastava, P. Saini, S. Raina, P. P. Ingole, R. Gupta and S. Sapra, *J. Phys. Chem. C*, 2015, **119**, 22690–22699.
18 Y. Yamada, T. Nakamura, M. Endo, A. Wakamiya and Y. Kanemitsu, *IEEE J. Photovoltaics.*, 2015, **1**, 401–405.
19 K. Wu, G. Liang, Q. Shang, Y. Ren, D. Kong and T. Q. Lian, *J. Am. Chem. Soc.*, 2015, **137**, 12792–12795.
20 L. Wang, C. F. Wu, H. Y. Wang, Y. F. Wang, Q. D. Chen, W. Han, W. P. Qin, J. McNeill and H. B. Sun, *Nanoscale*, 2013, **5**, 7265–7270.
21 J. S. Manser and P. V. Kamat, *Nat. Photonics*, 2014, **8**, 737–743.
22 Z. Y. Zhang, X. Chen, H. Y. Wang, M. Xv, B. R. Gao, Q. D. Chen and H.-B. Sun, *Phys. Chem. Chem. Phys.*, 2015, **17**, 30084–30089.
23 X. X. Wu, M. T. Trinh, D. Niesner, H. M. Zhu, Z. Norman, J. S. Owen, O. Yaffe, B. J. Kudisch and X. Y. Zhu, *J. Am. Chem. Soc.*, 2015, **137**, 2089–2096.
24 K. G. Stamplecoskie, J. S. Manserab and P. V. Kamat, *Energy Environ. Sci.*, 2015, **8**, 208–215.
25 H. Matsumoto, T. Matsunaga, T. Sakata, H. Mori and H. Yoneyama, *Langmuir*, 1995, **11**, 4283–4287.